PCCP

Accepted Manuscript

ROYAL SOCIETY OF CHEMISTRY

www.rsc.org/pccp

Journal Name Physical Chemistry Chemical Physics Dynamic Article Links ►

Cite this: DOI: 10.1039/c0xx00000x

www.rsc.org/xxxxxx

ARTICLE TYPE

The mechanism of $NaFePO_4$ (de)sodiation determined by in situ X-ray diffraction

Montserrat Galceran[a], Damien Saurel[a], Begoña Acebedo[a], Vladimir Roddatis[a], Egoitz Martin[a], Teófilo Rojo[a,b], Montse Casas-Cabanas*[a]

Received (in XXX, XXX) Xth XXXXXXXXX 20XX, Accepted Xth XXXXXXXXX 20XX
DOI: 10.1039/b000000x

The reaction mechanism occurring during the (de)intercalation of sodium into the host olivine $FePO_4$ structure is thoroughly analysed through a combination of structural and electrochemical methods. In situ XRD experiments have confirmed that the charge and discharge reaction mechanisms are different and have revealed the existence of a solid solution domain from $1 < x < 2/3$ in Na_xFePO_4 upon charge. The second part of the charge proceeds through a 2-phase reaction between $Na_{2/3}FePO_4$ and $FePO_4$ with strongly varying solubility limits. The strong cell mismatch between $Na_{2/3}FePO_4$ and $FePO_4$ enhances the effects of the diffuse interface and therefore varying solubility limits are first observed here in micrometric materials.

Introduction

Recent progress in the field of Na-ion batteries (SIBs) is endorsing the potential of this technology as a viable alternative to Li-ion batteries (LIBs) in the mid-term, particularly for stationary applications [1]. The numerous studies devoted to materials for SIBS in the last couple of years, among which the promising report of several full cells with honourable energy densities [2, 3, 4], is a clear sign of the quick development of this reborn research field after almost a three-decades break owing to the eclipsing success of LIBs.

There are however several aspects of Na-ion chemistry that remain to be understood for the development of a competitive technology. Among these, one can cite the electrode/electrolyte reactivity [4, 5], or the reaction kinetics and mechanisms of numerous electrode materials. Although the mirror of Li-ion technologies can be used as a solid background for the research of viable Na-ion systems, important differences between the two systems are continuously being revealed. Examples of it are the poor insertion Na into graphite [6], the fact that Na^+ ions are too large to be accommodated in a compact lattice like the spinel framework [7, 8] or the different reaction mechanism of Sb with Na when compared to Li [2].

The olivine host structure is also a good example of the differences between Li and Na intercalation chemistry. Indeed, $NaFePO_4$ exhibits one of the highest reversible capacities reported up to date for a polyanionic cathode material [9] and maintains some of the exceptional features of its Li counterpart: reaction within a narrow voltage range inside the voltage stability window of the electrolyte, good stability and good cyclability. Numerous works devoted to the mechanism of $LiFePO_4$ have revealed that the 2-phase reaction usually observed in micrometric materials can turn into a complex phase transition mechanism that depends strongly on microstructure (size, morphology, defects) and that are still the source of exciting debate. For example, several works have shown evidence of the possibility of inter-particle lithium diffusion in multi-sized multi-particle systems (i.e. electrodes) in equilibrium, which leads to a suppression of interfaces and stabilizes into a mixture of lithiated and delithiated single-phase particles [10, 11, 12]. It has also been found that the reaction mechanism can switch from a two phase reaction to a single phase reaction through a non-equilibrium transformation path [13] by tuning the size and microstructure of the material [14]. The ensemble of the works related to this active field, recently thoroughly reviewed by Malik et al. [15], is key to identifying the origin of the excellent rate performance this material exhibits and represent a step forward towards the understanding of electrochemical systems based on intercalation reactions.

Conversely, very little is known about the mechanism of the sodium system despite some noticeable differences from $LiFePO_4$ have already been reported. Contrary to the symmetrical biphasic mechanism observed in micrometric $LiFePO_4$ [16], Na extraction occurs in two voltage plateaus separated by an intermediate phase Na_xFePO_4 ($x\sim2/3$), whereas three phases ($FePO_4$, $Na_{2/3}FePO_4$ and $NaFePO_4$) appear simultaneously during Na insertion [17]. Based on ex-situ XRD and TEM analysis, we attributed this asymmetry to the mechanical aspects of the transformation, in account of the strong volumetric mismatch that the two end members of the system exhibit (17.58% for $FePO_4/NaFePO_4$ compared to 6.9% for the Li counter-parts).

We report here new insights into the mechanism of Na insertion and extraction into $FePO_4/NaFePO_4$ based on a detailed in-situ X-ray diffraction study, from which interesting new features have been identified and are thoroughly analysed.

Experimental

Synthesis of NaFePO4

$NaFePO_4$/C has been synthetized after chemical delithiation and further sodiation of commercially available 6% carbon-coated $LiFePO_4$ of 800nm primary particle size. The chemical oxidation was performed by stirring a mixture of pristine $LiFePO_4$ using NO_2BF_4 (Sigma-Aldrich) as oxidizing agent in acetonitrile (Sigma-Aldrich) at room temperature. The reaction was carried out in a glove box under argon atmosphere (O_2 and H_2O ppm ≤ 5). After the reaction was completed the mixture was vacuum filtered and the delithiated collected powder washed with acetonitrile twice and dried under vacuum at 80 °C overnight. The obtained $FePO_4$ powder was chemically sodiated with NaI (Sigma-Aldrich) in acetonitrile under reflux in argon atmosphere. The Na/Fe ratio of the final $NaFePO_4$ compounds has been verified by ICP and found to be equal to 0.95 ±0.03.

Characterization techniques.

For XRD measurements, Cu kα radiation was used on a Brüker D8 Advance X-ray diffractometer equipped with a LYNXEYE detector. For i*n situ* XRD experiments we have developed our own 22 mm inner diameter electrochemical cell, equipped with a Be window as current collector, operating in reflection geometry. Each scan was collected in 0.02° increments between 28° and 38° at a scanning speed of 0.018466° s^{-1}. The active material was prepared by mixing $NaFePO_4$/C with carbon (ketjen Black EC-600JD, Akzo nobel) in a ratio 80:20. About 25 mg of this mixture were placed into the cell against the Be window, below a Whatman GF/D borosilicate glass fiber sheet separator impregnated with 1.0 M sodium hexafluorophosphate ($NaPF_6$, Sigma-Aldrich) in ethylene carbonate (EC, Acros) : DMC (1:1 by volume) liquid electrolyte and high purity Na metal (Sigma-Aldrich) as anode. The cell was galvanostatically cycled at a current of 2.4 mA/g for a rate of C/66 using a SP200 Biologic potentiostat. Le Bail refinements were carried out with the FullProf program [18] (Windows version, May 2010).

Transmission electron microscopy (TEM) measurements were carried out by using a FEI Tecnai F20 electron microscope operated at 200 keV and equipped with High Angle Annular Dark Field (HAADF) detector and X-ray Dispersive Energy (EDX) spectrometer. The samples were ultrasonicated under acetone and the resulting dispersion of the powder was transferred to a quantifoil carbon film fixed on a 3 mm copper grid (200 mesh).

Results and discussion

The results of the in-situ XRD experiment of a $NaFePO_4$ electrode during the first cycle are presented in Figure 1. The top panel 1a presents the voltage vs. time curve, the central panel 1b displays a 2D plot of the diffraction patterns recorded along the electrochemical experiment and the bottom panel 1c displays the sum of the integrated intensity of the (020) and (211) peaks of $NaFePO_4$, Na_xFePO_4 (1<x<0) and $FePO_4$. As shown in figure 1a, the cell exhibits the typical asymmetrical voltage profile invariably found in this system [9, 19, 20, 17, 21]. Indeed, while upon discharge a single plateau is observed in the voltage-time curve, a voltage discontinuity is observed around x=0,7 on charge (blue dashed line in figure 1). This voltage discontinuity separates two rather constant voltage plateaus, typically associated with biphasic phase transformation mechanisms according to the Gibbs phase rule [22], and corresponds to the formation of an intermediate ordered phase as previously reported [9]. However, and despite a flat plateau is observed in PITT experiments before the voltage discontinuity as reported by Moreau *et al*. [9], a solid solution transformation mechanism is revealed here. Indeed, the reflections initially corresponding to $NaFePO_4$ continuously change in 2 theta position to reach the intermediate ordered phase $Na_{2/3}FePO_4$ at the voltage discontinuity (region I, figure 1b)).

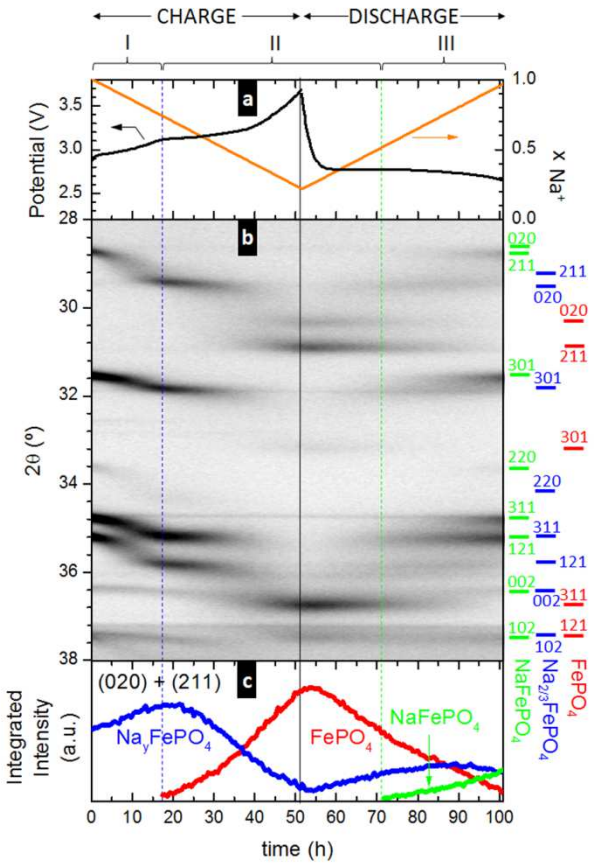

Figure 1. a) Voltage versus time curves of the XRD in situ experiment. b) 2theta versus time plot of the XRD patterns comprising a full cycle (charge and discharge). The level of grey indicates the relative intensity (the darker the more intense). Horizontal bars at the right indicate the position of the Bragg peaks for each of the phases involved. c) Sum of the integrated intensity of the (020) and (211) reflections for each of the phases involved versus time.

As can be seen in figure 1b and 1c, soon after the voltage discontinuity, $FePO_4$ reflections emerge as the amount of sodium decreases within the electrode. These reflections increase in intensity throughout the charge reaction and coexist with the vanishing reflections of the intermediate ordered phase $Na_{2/3}FePO_4$ until the end of charge. During the first part of discharge this mechanism is reversible, with a gradual decrease of $FePO_4$ peaks parallel to an increase of $Na_{2/3}FePO_4$ reflections. Therefore, in a broad region covering the second part of the charge reaction and the first part of the discharge (region II in

figure 1) the system displays a symmetrical biphasic transformation mechanism, similar to what is usually observed in the $LiFePO_4$ system (except that in the latter the reaction occurs between the end members $FePO_4$ and $LiFePO_4$). However, before reaching the middle of the discharge (region III of figure) $NaFePO_4$ starts forming as more sodium is inserted into the system, although $FePO_4$ and $Na_{2/3}FePO_4$ reflexions are still observed. The main feature of the end of charge is thus the simultaneous presence of 3 phases, in accordance with our previous observations in ex-situ XRD patterns of partially discharged electrodes [17].

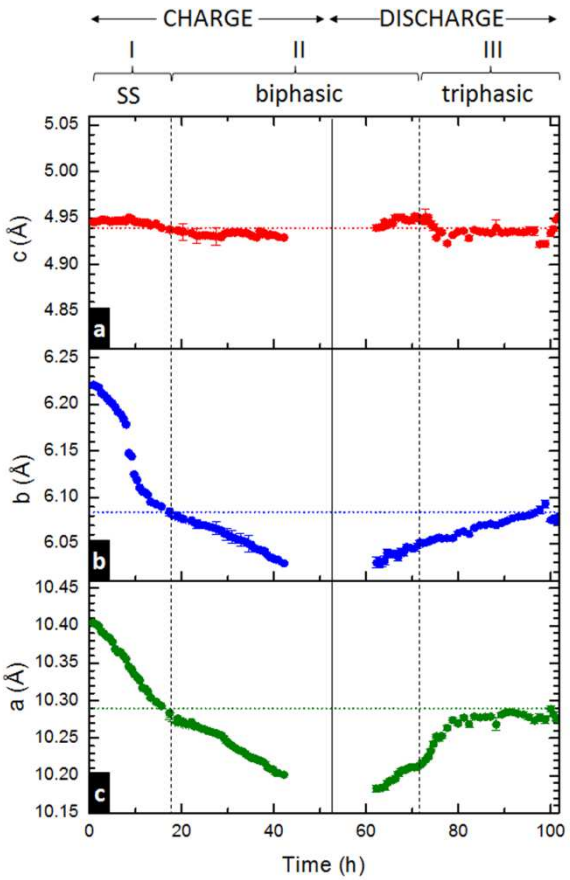

Figure 2. Evolution of the cell parameters of Na_yFePO_4 during charge and discharge of the battery. The size of the symbols is approximately the size of the error. The dotted horizontal lines indicate the cell parameters of the chemically synthesized intermediate ordered phase $Na_{2/3}FePO_4$ as previously reported [17]. The plain vertical line indicates end of charge, and the two dashed vertical lines indicate the limit of the regions with different mechanisms.

The evolution of the cell parameters for the sodium rich phase, obtained from Le Bail's refinements of each XRD, is displayed in figure 2 (see supporting information for more details). The cell parameters of all involved phases have been refined in all patterns together with profile parameters and background parameters. Although the intermediate phase is known to exhibit a superstructure, the cell parameters and the space group of the subcell have been used for simplicity throughout the whole experiment. The values between the end of charge and beginning of discharge are not plotted as the low intensity of the peaks prevented their reliable estimation. The lattice parameters found for the end members, $NaFePO_4$ at beginning of charge (a = 10.393(1) Å, b = 6.207(6) Å and c = 4.9335(8) Å) and $FePO_4$ at the end of charge (a = 9.7989(9) Å, b = 5.7962(4) Å, c = 4.806(2) Å), are in accordance with previously reported values for these phases [9, 17]. As was observed from the 2D plot of figure 1b, the solid solution mechanism can be clearly identified in figure 2c by the linear decrease of the unit cell parameter a at the beginning of charge in accordance with Vegard's empirical law [11] until the cell parameters of the $Na_{2/3}FePO_4$ phase are obtained at the voltage discontinuity (a = 10.284(1) Å, b = 6.0848(7) Å and c = 4.9381(7) Å), also indicated by the horizontal dot lines in figure 2. The evolution of the cell parameter b is completely different as it begins decreasing linearly but drops abruptly well before the voltage discontinuity, indicating a drastic shrinking of the unit cell. This finding might suggest that the ordering starts to take place before the composition $Na_{2/3}FePO_4$ is actually reached. Unexpectedly, beyond the voltage discontinuity, and concomitant to the appearance of $FePO_4$, the cell parameters a and b of the intermediate phase are not constant as would be expected in a two-phase reaction but rather continue evolving linearly with a reduced slope. Therefore Na_yFePO_4 compositions are formed with y<2/3, and reach limit cell parameter values of a = 10.197(4) Å, b = 6.026(4) Å and c = 4.911(2) Å around x = 0.3 (note that from now on x is used to define the average Na content in the electrode and y to define the average content of Na in the Na-rich phase, Na_yFePO_4). Assuming that the change of slope in the evolution of cell parameters is entirely due to the simultaneous formation of $FePO_4$, an extrapolation of the linear dependence of the parameter a before the voltage discontinuity leads to a sodium content close to y = 0.5 in Na_yFePO_4 at the end of charge. Therefore the solubility limit of the Na-rich phase would be $Na_{0.5}FePO_4$ for x = 0.3. The cell parameters of $FePO_4$ also evolve slightly (not plotted), as will be shown below.

Cell parameters	Mismatch (%)			
	$FePO_4$ vs $LiFePO_4$	$FePO_4$ vs $NaFePO_4$	$FePO_4$ vs $Na_{2/3}FePO_4$	$Na_{2/3}FePO_4$ vs $NaFePO_4$
a	5.1	5.9	4.7	1.1
b	3.7	7.4	5.0	2.3
c	1.9	3.4	3.3	0.2
Volume	6.9	17.6	13.5	3.6

Table 1. Cell mismatch (in %) between the coexisting phases in $LiFePO_4$ and $NaFePO_4$ systems, for individual crystalline directions and total volume.

Upon discharge, the cell parameter b of Na_yFePO_4 also evolves quite symmetrically to the end of charge, increasing linearly despite two phases are present. At the end of discharge, when $FePO_4$ has almost disappeared, the value corresponding to the intermediate phase $Na_{2/3}FePO_4$ is reached. Curiously, the cell parameter a increases faster than b and reaches the value of the intermediate phase $Na_{2/3}FePO_4$ around the middle of discharge. Remarkably, neither a nor b go beyond the value of the

intermediate phase upon charge. Finally, cell parameter *c* is almost constant during the whole charge/discharge cycle, as was predictable in regard of the very low mismatch between the Na-rich phases along this direction (table 1).

In order to get more insight into the solid solution mechanism and verify these compelling results, the evolution of two individual reflections, $(301)_{Na_yFePO_4}$ and $(020)_{FePO_4}$, has been thoroughly examined upon charge. Both peaks are well isolated from others, even in the simultaneous presence of both materials, making them good independent probes for the evolution of the two phases. Since the cell parameter *c* has been found to vary only slightly in Na_yFePO_4, it can be considered that most changes in the position of reflection $(301)_{Na_yFePO_4}$ arise from the cell parameter *a*. A lorentzian fit has been used in order to extract the evolution of their position and full width at half maximum (FWHM), both shown in figure 3. The peak position of reflection $(301)_{Na_yFePO_4}$ is found to constantly shift towards higher angles, indicative of a decrease in cell parameters. This evolution follows a linear trend with a change of slope at the voltage discontinuity, in good agreement with the evolution of the cell parameter *a* of Na_yFePO_4 plotted in figure 2, and confirms the continuous variation in composition of the Na-rich phase throughout the whole reaction. The same behaviour is observed for $(020)_{FePO_4}$ reflection, which is shown to move towards larger angles as sodium content in the electrode decreases. This demonstrates that the solubility limits vary with concentration both for the Na-rich (Na_yFePO_4) and the Na-poor ($FePO_4$) phases.

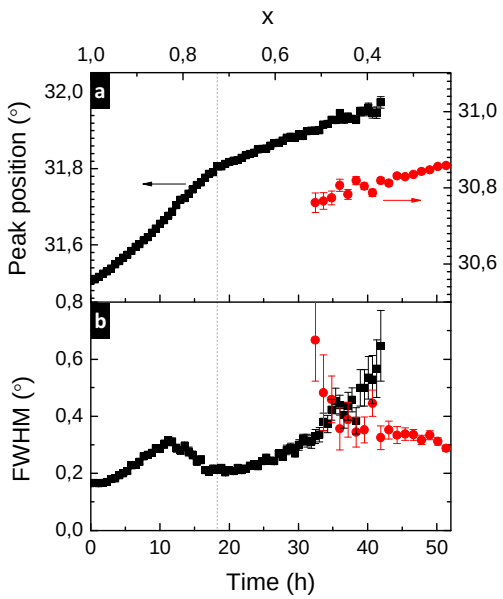

Figure 3. Evolution of $(301)_{Na_yFePO_4}$ and $(020)_{FePO_4}$ reflections during the charge reaction. a) Peak position, b) FWHM (°). The dotted horizontal line indicates the voltage discontinuity.

Regarding the evolution of the FWHM of $(301)_{Na_yFePO_4}$ reflection, a rapid increase is found at the beginning of charge within the solid solution domain (corresponding to region I in figure 1 a)). Since no interface between different compositions has been formed yet, this result indicates that the extraction of Na induces coherency strains. These are probably derived from the presence of a small gradient of sodium concentration within the crystalline phase which in turn suggests that the system does not have the time to homogenise the bulk concentration during Na extraction. A maximum is reached around x=0.85 after which the FWHM of $(301)_{Na_yFePO_4}$ starts to decrease to reach a minimum at the voltage discontinuity because of the accommodation of strains that results from the ordering of sodium and vacancies. This would support the hypothesis that the ordering occurs before the composition $Na_{2/3}FePO_4$ is actually reached. Above the voltage discontinuity and while the amount of $FePO_4$ starts increasing, the FWHM of the Na-rich phase increases again considerably, reaching even higher values than in the first part. Diverse factors can be invoked to explain this observation, the overall FWHM being probably the result of their combination. On one hand, the decrease of Na content in Na_yFePO_4 might result again in an increase in coherency strains. Moreover, the presence of an interface between the sodium-rich and sodium-poor phases would also lead to an increase of coherency strains and a reduction of domain size for the vanishing phase. This factor is further supported by the FWHM reduction of $(020)_{FePO_4}$ peak, shown as well in figure 3b, which is expected to follow the inverse evolution as the biphasic transformation proceeds and the size of $FePO_4$ domains increases. Finally, since the initial FWHM of $(301)_{Na_yFePO_4}$ reflection is not completely recovered at the end of charge, the volume reduction derived from Na removal could also result in textural transformations to accommodate the strains, leading to a mosaic texture and finally to crack formation, both resulting in a reduced size of the crystallites.

TEM has been used to characterise a sample that was stopped in the vicinity of the voltage discontinuity upon charge after six cycles. Figure 4a shows a low magnification image of the different particles, where it can be seen that all the particles are uniformly surrounded by carbon black. Many particles exhibit well developed cracks which are typical macroscopic defects formed in olivine-phosphates during Li^+ insertion or extraction [23]. Overall the amount of cracks is now larger than previous to cycling and partial fragmentation of the original $NaFePO_4$ particles can indeed be observed. Figure 4b shows an interface between two crystalline domains corresponding to Na_yFePO_4 ($y\approx2/3$) and $FePO_4$, according to the ratio of the interlayer distances along *b* direction. Note that a different contrast perpendicular to [120] direction can be observed in the lower domain due to Na/vacancy ordering. In figure 4c the superposition of the Fourier Transform of each of the domains is shown. Red spots originate from the $FePO_4$ domain, green from Na_yFePO_4 ($y\approx2/3$) and yellow results from the superposition of both. These two images further confirm that the 2 phases coexist within the particles and, interestingly, the interface between the two materials is found along *ac* plane. This observation is in contrast with what occurs with $LiFePO_4$, for which the interface has been reported to occur usually along the *bc* plane because contains the lower mismatch strains (see table 1) and allows minimizing coherency strains by keeping the largest mismatch direction out of the interface [24]. In the case of an interface between Na_yFePO_4 and $FePO_4$, while the lowest mismatch is also along *c*, the mismatch along *a* and *b* directions is very close, although slightly higher along *b* (4.67% and 4.98%, respectively). The energy difference between an interface along *ac* or *bc* will be low and might even change with the extent of reaction. We thus expect the orientation of the interface to be easily affected by

other factors such as kinetics or history of the sample. In this case the interface we observe is the most favourable in terms of mismatch (*ac*), which might additionally be kinetically favoured. Indeed, the interface orientation will be kinetically more facile

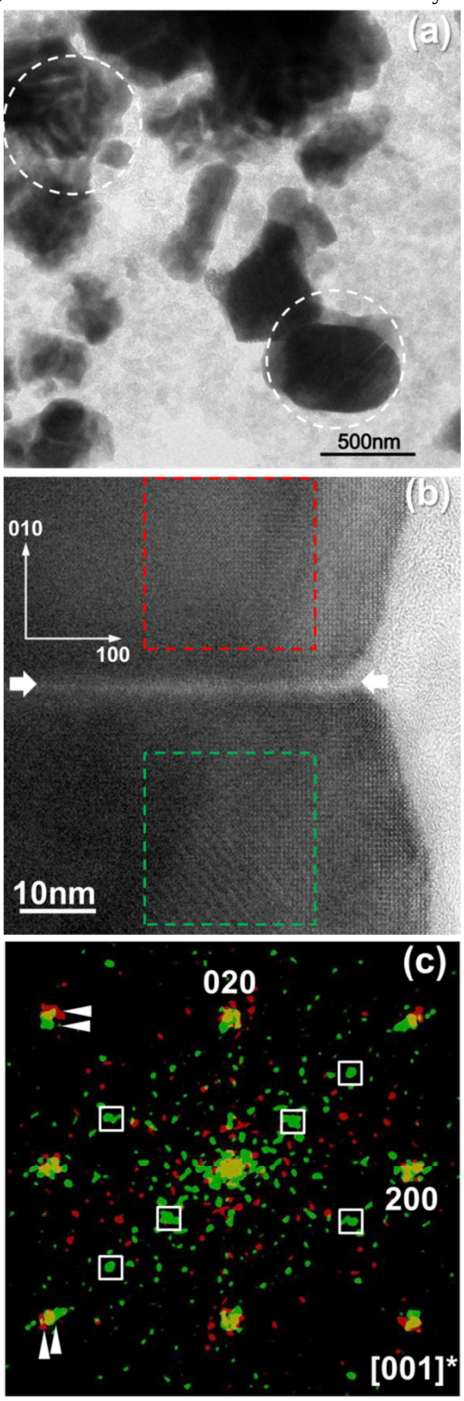

Figure 4. a) Low magnification TEM image of a material stopped during charge after 6 cycles where areas with cracks are highlighted. b) High magnification image of [001] zone axis where a domain boundary can be observed between Na-rich and Na-poor phases. c) Superposition of Fourier transform from the top and from the bottom of the image, presenting a splitting of the diffraction spots. Superstructure spots corresponding to Na_yFePO_4 (y≈2/3) are marked with squares.

perpendicular to the direction of Na^+ transport [24], e.g. *b* as in $LiFePO_4$ [13, 25]. The same could apply to the interface between $NaFePO_4$ and Na_yFePO_4 although in this case the cell mismatch is much lower and a larger difference is observed between both directions.

Several complex new features in the reaction mechanism between $NaFePO_4$ and $FePO_4$ have been shown in this study. In addition to the asymmetric reaction path between charge and discharge, a solid solution range between x=1 and x= 2/3 and a variation of Na^+ solubility as a function of its overall concentration in the 2-phase and 3-phase regions of the electrochemical curve has been revealed. Interestingly, varying solubility limits have been predicted [26] and recently reported for nanosized $LiFePO_4$ [27, 28, 29, 30]. Based on the seminal work of Burch *et al.* [31], in which a contraction of the miscibility gap with particle size reduction to the scale of the diffuse interface thickness between Li rich and Li poor phases was shown, Wagemaker *et al*. concluded that the change in phase domain size with composition also results in compositional changes within each phase [28]. However, these effects are observed in $LiFePO_4$ nanoparticles with dimensions below 100nm, while the primary particle size of our pristine material is around 800 nm. On the other hand the two systems significantly differ in lattice mismatch of the end members (6.87% in volume for $LiFePO_4/FePO_4$ and 13.48% in volume for $Na_{2/3}FePO_4/FePO_4$ as shown in table 1). Lattice mismatch has a dual effect in the free energy of mixing; it contributes to the gradient penalty of the interface, leading to more extended interfaces, and to the elastic stress generated by the two-phase coexistence. The result is that an enhanced effect is observed when the cell mismatch is large. What occurs in the 3-phase domain is however more difficult to decipher, and probably depends on dynamics and kinetics. Resolving such a question will require additional theoretical and experimental work.

The results shown here witness of the impact of interface effects and open the door to a systematic investigation of the particle size dependence of Na insertion into $FePO_4$. Moreover, similar behaviours are also expected in other Na intercalation materials operating at room temperature through a two-phase process with the end members having a large unit cell mismatch. The notable differences in the reaction mechanism found here between $LiFePO_4$ and $NaFePO_4$ are reminders that the simple transfer of Li-ion technology to Na-ion systems would be an oversimplification. Detailed knowledge of the transformation mechanisms occurring will be key for the development of improved SIB materials, as has been shown in LIB technology.

Conclusions

The mechanism of $NaFePO_4$ battery material has been thoroughly analysed by in situ X-ray diffraction. This study has confirmed that the typical asymmetrical voltage profile of the $FePO_4/NaFePO_4$ system results from a different reaction path. Sodium is extracted from $NaFePO_4$ through a single homogeneous phase process until the intermediate phase $Na_{2/3}FePO_4$ forms at the voltage discontinuity. This process is accompanied by a drastic reduction of the cell parameter *b* and accommodation of coherency strains as a result of Na/vacancies ordering. Further sodium extraction occurs in a 2-phase process between a Na-rich Na_yFePO_4 phase and a Na-poor $FePO_4$ phase

whose composition has been found to vary with overall Na content in the electrode. More complex is the discharge reaction, with the simultaneous presence of three phases with varying miscibility limits. Diffuse interfaces between different phases are considered accountable of their varying average composition, enhanced here by the stress caused by a large cell mismatch. The remarkable consequence of these findings is that diffuse interfaces will have a higher impact in Na-ion than in Li-ion intercalation chemistry. Indeed, a reduced miscibility gap, strongly dependent on the overall composition, has here been found in micrometric materials.

Acknowledgements

The authors would like to thank the Basque Government for financial support through Etortek project energiGUNE'10 and A. Saracibar and M. Armand for helpful discussions.

Notes and references

[a]*CIC ENERGIGUNE, Parque Tecnológico de Álava, Albert Einstein 48, ED.CIC, 01510, Miñano, Spain; Tel: +34 945297108; E-mail: mcasas@cicenergigune.com*

[b]*Departamento de Química Inorgánica, Universidad del País Vasco UPV/EHU, P.O. Box. 644, 48080, Bilbao, Spain. Fax: +34 946013500; Tel: +34 946012458.*

† Electronic Supplementary Information (ESI) available: Evolution of the diffraction XRD patterns through the in situ experiment with selected examples of Le Bail fits. See DOI: 10.1039/b000000x/

1. V. Palomares, P. Serras, I. Villaluenga, K. B. Hueso, J. Carretero-Gonzalez, and T. Rojo, *Energy & Environmental Science*, 2012,**5**(3),5884.
2. K. Chihara, A. Kitajou, I. D. Gocheva, S. Okada, and J. Yamaki, *Journal of Power Sources*, 2013, **227**,80.
3. D. Kim, E. Lee, M. Slater, W. Q. Lu, S. Rood, and C. S. Johnson, *Electrochemistry Communications*, 2012, **18**, 66.
4. A. Ponrouch, R. Dedryvere, D. Monti, A.E. Demet, J.M. Ateba Mba, L. Croguennec, C. Masquelier, P. Johansson, and M.R. Palacin, *Energy Environ. Sci.*, 2013, **6**, 2361.
5. S. Komaba, W. Murata, T. Ishikawa, N. Yabuuchi, T. Ozeki, T. Nakayama, A. Ogata, K. Gotoh, and K. Fujiwara, *Advanced Functional Materials*, 2011, **21**(20), 3859.
6. D. A. Stevens and J. R. Dahn, *Journal of the Electrochemical Society*, 2001, **148**(8), A803.
7. Y. Sun, L. Zhao, H. Pan, X. Lu, L. Gu, Y-S. Hu, H. Li, M. Armand, Y. Ikuhara, L. Chen, and X. Huang, *Nat Commun*, 2013, **4,** 1870.
8. N. Yabuuchi, M. Yano, S. Kuze, and S. Komaba, *Electrochimica Acta*, 2012, **82**, 296.
9. P. Moreau, D. Guyomard, J. Gaubicher, and F. Boucher, *Chemistry of Materials*, 22(14):4126–4128, July 2010.
10. C. Delmas, M. Maccario, L. Croguennec, F. Le Cras, and F. Weill, *Nature Materials*, 2008, **7**(8), 665.
11. K. T. Lee, W. H. Kan, and L. F. Nazar, *Journal of the American Chemical Society*, 131(17):6044–+, May 2009.
12. W. Dreyer, J. Jamnik, C. Guhlke, R. Huth, J. Moskon, and M. Gaberscek, *Nature Materials*, 2010, **9**(5),448.
13. R. Malik, F. Zhou, and G. Ceder, *Nature Materials*, 2011, **10**(8), 587.
14. P. Gibot, M. Casas-Cabanas, L. Laffont, S. Levasseur, P. Carlach, S. Hamelet, J. M. Tarascon, and C. Masquelier, *Nature Materials*, 2008, **7**(9),741.R. Malik, A. Abdellahi, and G. Ceder, *Journal of the Electrochemical Society*, 2013, **160**(5), A3179.
15. R. Malik, A. Abdellahi, and G. Ceder. A critical review of the li insertion mechanisms in lifepo4 electrodes. *Journal of the Electrochemical Society*, 160(5):A3179–A3197, 2013.
16. A. K. Padhi, *K. S. Nanjunda*swamy, a**nd** J. B. Goodenough, *Journal of the Electrochemical Society*, 1997, **144**(4), 1188.
17. M. Casas-Cabanas, V. V. Roddatis, D. Saurel, P. Kubiak, J. Carretero-Gonzalez, V. Palomares, P. Serras, and T. Rojo, *Journal of Materials Chemistry*, 2012, **22**(34), 17421.
18. J. Rodríguez-Carvajal, *Physica B: Condensed Matter*, 1993, 192, 55.
19. K. Zaghib, J. Trottier, P. Hovington, F. Brochu, A. Guerfi, A. Mauger, and C. M. Julien. *Journal of Power Sources, 2011*, **196**(22), 9612.
20. S.-M. Oh, S.-T. Myung, J. Hassoun, B. Scrosati, and Y.-K. Sun. *Electrochemistry Communications*, 2012, **22**, 149.
21. Y. Zhu, Y. Xu, Y. Liu, C. Luo, and C. Wang. *Nanoscale*, 2013, **5**(2), 780.
22. G-A. Nazri, C. Julien, editor. *Solid State Batteries: Materials Design and Optimization*. Kluwer, 1997.
23. G. Chen, X. Song, and T.J. Richardson. *Journal of The Electrochemical Society*, 2007, **154**(7), A627.
24. A. Van der Ven, K. Garikipati, S. Kim, and M. Wagemaker. *Journal of The Electrochemical Society*, 2009, **156**(11), A949.
25. R. Tripathi, S. M. Wood, M. S. Islam, and L. F. Nazar. *Energy Environ. Sci.*, 2013, **6**, 2257.
26. M. Wagemaker, F.M. Mulder, and A. Van der Ven, *Advanced Materials*, 2009, **21**(25-26), 2703.
27. N. Meethong, Y-H. Kao, M. Tang, H-Y. Huang, W. C. Carter, and Y-M. Chiang, *Chemistry of Materials*, 2008, **20**(19), 6189–6198.
28. M. Wagemaker, D.P. Singh, W.J.H. Borghols, U. Lafont, L. Haverkate, V.K. Peterson, and F.M. Mulder, *Journal of the American Chemical Society*, 2011, **133**(26), 10222.
29. N. Sharma, X. Guo, G. Du, Z. Guo, J. Wang, Z. Wang, and V.K. Peterson, *Journal of the American Chemical Society*, 2012, **134**(18), 7867.
30. Y. Orikasa, T. Maeda, Y. Koyama, H. Murayama, K. Fukuda, H. Tanida, H. Arai, E. Matsubara, Y. Uchimoto, and Z. Ogumi, *Chemistry of Materials*, 2013, **25**(7), 1032.
31. D. Burch and M.Z. Bazant, *Nano Letters*, 2009, 9(11), 3795.

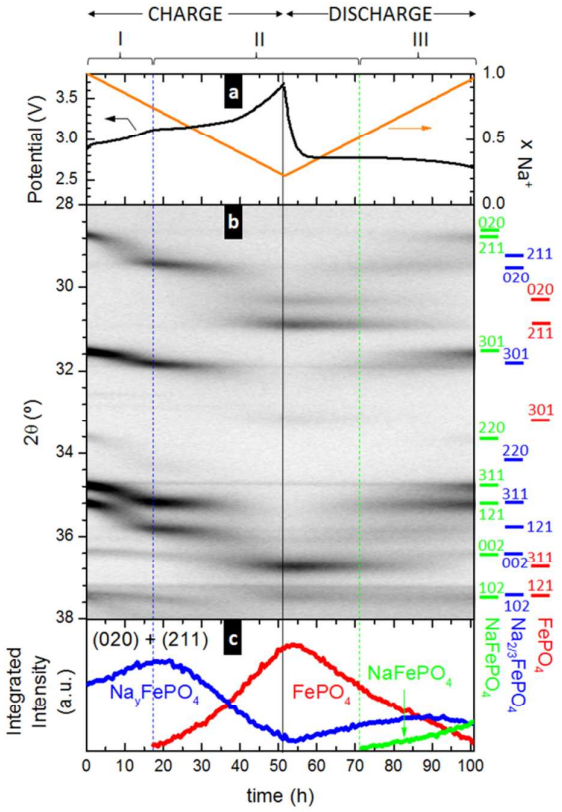

Insight into the mechanism of Na insertion and extraction into $FePO_4/NaFePO_4$ based on a detailed in-situ X-ray diffraction study, from which interesting new features were identified and analysed.